Meccanica (2024) 59:1577–1592
https://doi.org/10.1007/s11012-024-01856-5

RESEARCH

# A method to enhance the nonlinear magnetic plucking for vibration energy harvesters

**Michele Rosso · Simone Cuccurullo · Filippo Pietro Perli · Federico Maspero · Alberto Corigliano · Raffaele Ardito**

Received: 25 April 2024 / Accepted: 10 July 2024 / Published online: 2 August 2024


**Abstract** In this work, a technique to improve the magnetic plucking for frequency up-conversion in piezoelectric energy harvesters is presented. The technique involves shielded magnets with Neodymium-iron-boron alloy polarized in the opposite direction on a main magnet. The phenomenon is investigated both at the computational and at the experimental level. Subsequently, simulations on a mesoscale piezoelectric energy harvester are presented which demonstrate a gain of 17 times if the magnets are shielded in comparison with the classical plucking (i.e. without shielding). The technique finds useful applications and benefits in the field of low-speed and low-frequency vibration energy harvesting, as well as in actuation and sensing.

**Keywords** Vibration energy harvesting · Nonlinear dynamics · Magnetic plucking · Frequency up-conversion · Flux concentrator

M. Rosso (✉) · F. P. Perli · A. Corigliano · R. Ardito
Department of Civil and Environmental Engineering, Politecnico di Milano, Piazza Leonardo da Vinci, Milano 20133, Italy
e-mail: michele.rosso@polimi.it

F. P. Perli
e-mail: filippopietro.perli@polimi.it

A. Corigliano
e-mail: alberto.corigliano@polimi.it

R. Ardito
e-mail: raffaele.ardito@polimi.it

S. Cuccurullo · F. Maspero
Department of Physics, Politecnico di Milano, Piazza Leonardo da Vinci, Milano 20133, Italy
e-mail: simone.cuccurullo@polimi.it

F. Maspero
e-mail: federico.maspero@polimi.it

## 1 Introduction

Vibration-based energy harvesting (VEH) consists in collecting kinetic energy from mechanical vibrations of the surroundings and converting it into electrical energy. In the last two decades, VEH has drawn attention because it is a valuable option to extend the durability of batteries for portable electronics and, possibly, to introduce self-powering devices. The proposed energy conversion mechanisms are based on piezoelectric materials [1], electromagnetic generators [2], and electrostatic interaction [3]. In particular, piezoelectric harvesters have received the most attention because they allow for a direct conversion from kinetic to electrical energy, leading to larger power densities and a more straightforward integration in micro-power sources [4, 5]. In recent years, researchers have been exploring the performance of biocompatible, non-toxic piezoelectric materials in order to develop environmentally friendly applications [6].

Typical vibration sources cover a frequency bandwidth that goes from few Hz (human walking or running) to hundreds of Hz (domestic and industrial

machinery) [7]. Even though several groups have proposed to work at resonance with environmental vibrations [8], this is not the most viable option from the perspective of electromechanical conversion efficiency. Indeed, the energy harvested at low frequencies (1–100 Hz) is not enough to power microsystems [9]; moreover, the frequency of ambient vibrations can vary significantly over time.

A strategy to overcome these limitations is the frequency up-conversion mechanism [9–11]: low-frequency environmental vibrations are converted into high-frequency vibrations of the harvester, which can work at their resonance frequency to optimize the electromechanical conversion efficiency. Several frequency up-converting devices are based on the plucking mechanism, which consists in the deflection and the release of the harvester, e.g. a piezoelectric cantilever, to excite a high-frequency vibration. The plucking mechanism is obtained either by mechanical contact or by magnetic interaction. In the first case, a piezoelectric beam is put in free oscillations when plucked by a plectrum [12], by notches on a moving structure [13] or by a sliding mass [14]. In the other case, a permanent magnet (PM) deflects and releases a magnetized harvester through contactless magnetic interaction; both repulsive and attractive configurations have been studied [15, 16], as well as both rotational [17–19] and traslational mechanisms [20, 21]. The advantage of magnetic plucking is the absence of contact on the brittle piezoelectric material; indeed, damages due to wear worsen the conversion efficiency of the piezoelectric beam [22]. However, long-range magnetic interaction could hinder a proper release phase, which ideally should be as sharp as possible to excite high-frequency vibrations of the harvester; for this reason, very high plucking velocities are needed to maximize the efficiency [22]. Therefore, this aspect can represent a significant operational limitation for harvesters in the context of low-speed applications (less than 1 m/s), such as those related to human motion. Although, as previously described, the application of magnetic plucking has been widely exploited, the possibility of enhancing the frequency up-conversion process through the engineering of the magnetic force to make the interaction more impulsive has not been explored.

The aim of this paper is to propose a novel technique for manipulating magnetic plucking, and thus to improve its impulsiveness. Our idea is to shield one or both permanent magnets with other magnets of opposite polarity, in order to alternate attractive and repulsive force regimes, and sharpening the release step. The detailed description of our idea is presented in the Sect. 2 of this article. Subsequently, in Sect. 3, we provide an analytical model, numerical simulations to highlight the advantage of the proposed technique, and experimental validation using a custom setup. In Sect. 4, we apply the technique to energy harvesting, simulating a meso-scale case study. We show that, by properly adjusting the thickness of the shielding, a significant amplification in the plucking dynamics (i.e., displacement-velocity portrait of the harvester) can be achieved. Closing remarks are provided in Sect. 5.

## 2 Technique description

The basic idea for magnetic field manipulation is to exploit a device called *magnetic flux concentrator* (MFC) appropriately placed in the source region of the magnetic field. The MFC is essentially a block of suitably shaped soft ferromagnetic material. The principle of operation is based on the high magnetic permeability of such a material, which forces the flux lines in the surrounding space to follow the path indicated by its own geometry. The field lines are then free to expand into spatial regions where the permeability remains low, giving rise to an engineered pattern of the magnetic field. An illustration of this principle is shown in Fig. 1a with reference to an inductor for electromagnetic heat treatments. Researchers also used this principle recently, to improve the gap-to-gap heating of wind power gear [23], to control heating cycles at high temperatures [24] or in hot stamping steel sheets [25]. Gao et al. [26] in 2016 focused on studying the effect of geometric size on concentrator performance. In the MEMS field generally, flux concentrators are instead used to increase sensitivity and to redirect the field in Hall effect sensors. A study of general application on the material and shape was made in 2013 by Sun et al. [27]. Maspero et al. [28] recently made a MEMS magnetometer with flux concentrators. As an alternative to the flux concentrator, it is possible to use the patterned deposition of magnetic material [29] via the high-rate deposition triode sputtering technique.

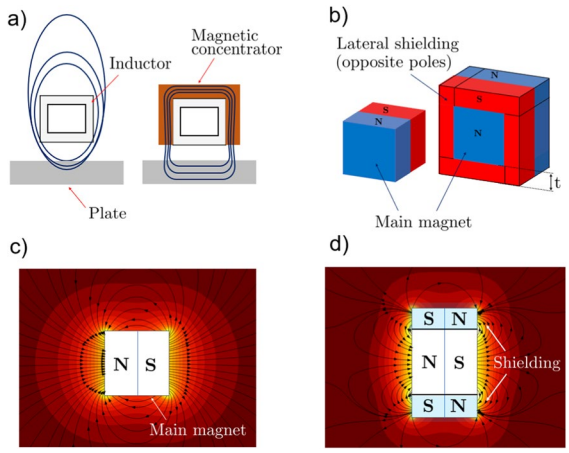


**Fig. 1** Schematic of MFC application (**a**), and similar application with polarized material on permanent magnets (**b**). Illustration of the typical contour plot of the magnetic field magnitude and magnetic field lines for the unshielded (**c**), and shielded (**d**) magnet

In this work, a similar concept to the MFC is applied, with a specific application to frequency up-conversion via magnetic plucking in piezoelectric vibration energy harvesters. The idea is similar to manipulate the flux lines of the magnetic field generated by the permanent magnets in the harvesting system using additional material around them, as explained in detail below. The motivation, as previously mentioned, lies in the fact that it is not always possible to have an impulsive phenomenon on the harvester in the operational context of low-frequencies and velocities (e.g. human motion). The MFCs are applied to an energy harvester consisting of two dynamical systems: a bimorph piezoelectric cantilever beam and a moving mass along a predefined path transversal to the beam's longitudinal axis, as will be shown in Sect. 4. Both the beam and the mass are equipped with cuboidal permanent magnets, enabling reciprocal interaction through magnetic force. This interaction occurs as the moving mass gets close to the cantilever tip through a low-frequency input vibration in a real frequency up-conversion system. If the velocity of the interaction between the PMs is very low, the plucking of the harvester does not occur due to the long-range nature of the magnetic force [30], and only a quasi-static phenomenon is observed without significant energy conversion. The main goal of this study is to increase the impulsiveness of the magnetic interaction by sharpening the magnetic force between the equipped magnets with respect to their relative distance. To achieve it, the four sides of the so-called main PMs parallel to the magnetization direction (4 over 6 faces in a parallelepiped case) are covered with additional PMs having an inverted polarization, as depicted in Fig. 1b. The main difference between MFCs and PMs is that MFCs are soft materials that become magnetized with respect to the magnetic field to which they are subjected. PMs, on the other hand, have a fixed magnetization and for high coercive fields, are not affected by an external field. The choice of using PMs to carry out the shielding derives from preliminary analyses in which greater efficiency was noted in the shaping of the plucking compared to the case of the soft material. Such a fact is due to the high capability of the PM to mantain constant the magnetization. It is also shown that by covering both or just one of the main PMs the technique still maintains its validity. The case with only one shielded magnet is studied both for completeness of investigation and because its effectiveness can be highly useful in scenarios where the same harvester is to be used, without altering the original tip mass, in different contexts of velocities and acceleration. In such a scenario, the magnetization arrangement on the moving magnet can be changed in the device without directly intervening on the harvester, thus avoiding the risk of damaging. In the Fig. 1c, d, the contour plot of the magnetic field and the magnetic field lines are shown for the unshielded and shielded cases, respectively, based on our finite element analyses. As it can be seen, for the shielded magnet (Fig. 1d) the magnetic field is more localized around its geometry, in comparison with the unshielded magnet (Fig. 1c). All the PMs in the systems are made of Neodymium-Boron-Iron alloy (NdFeB). These magnets have a higher magnetic energy density compared to ferrite magnets, allowing for the use of very small magnets, which are useful for creating highly compact systems. Additionally, their magnetic field intensity ensures sufficiently high interaction forces. The advantages have favored their selection since the early studies in this field [31].

## 3 Investigation

### 3.1 Modeling

In this section, the magnetic force modeling strategy is briefly recalled. The multi-dipole analytical approach [32], and the finite element method (FEM)

are used. The analytical formula, that has been provided by Yonnet and coworkers in the 80's, is valid for cuboidal permanent magnets, in which the magnetization is uniform and rigid. With reference to Fig. 2a, the formula that computes the i-component of the magnetic force reference system is the following:

$$F_i = \frac{\mathbf{J}\cdot\mathbf{J}'}{4\pi\mu_0} \sum_{m,n,p,q,r,s=0}^{1} (-1)^{m+n+p+q+r+s}\cdot\phi_i(U_{mn},V_{pq},W_{rs},R) \tag{1}$$

where $\mathbf{J}$ and $\mathbf{J}'$ are the magnetization vectors expressed in Tesla, $\mu_0$ is the magnetic permeability of vacuum equal to $4\pi\cdot10^{-7}$ H/m. The parameters $m$, $n$, $p$, $q$, $r$, $s$ are related to the corners of the two magnets. They can be equal to 0 or 1. The combinations of $m$, $p$, $r$ identifies the corner of one magnet and $q$, $r$, $s$ of the other. The coefficients $\phi_i$ that appear in (1), depend on four coefficients, which can be computed on the basis of geometric features namely (see Fig. 2a): $a$, $b$, $c$, half-lengths of the sides of one magnet; $A$, $B$, $C$, half-lengths of the sides of the other magnet; $\alpha$, $\beta$ and $\gamma$ relative distance components between the centroids of the magnets. The details of the formulas are reported in [32, 33].

The analytical formula is suitably modified to account for the presence of shielding magnets. Each magnet is treated separately and the interactions with all other magnets is considered. The hypotesis of permanent, rigid, and parallel magnetization is assumed. The FEM simulations are developed with the commercial software COMSOL Multiphysics®. A fully 3D model, with tetrahedral quadratic elements, has been developed in the framework of the magnetostatics module. The procedure works by computing first a magnetic potential, and then Lorentz's force with no electric fields. As experienced for the case without shielding [34], the FE simulations on a computer (16 GB RAM and core i7) require hours of calculation, while the Yonnet formula few milliseconds, with the same level of accuracy.

### 3.2 Simulations and experimental results

The magnets are Neodymium–Iron–Boron cubes with a side of 3 mm, and a magnetization value of 1.32 T. The shielding, on the other hand, is made by placing parallelepiped plates of the same material and magnetization, with a volume of $1\times3\times4\,\text{mm}^3$, next to the main magnet, as indicated in the schematic of Fig. 1b. The investigation is conducted by comparing the interaction force between the two magnets without shielding with the case with both shielded magnets or just one.

In particular, the reference framework for evaluating the magnetic force is depicted in Fig. 2b. One of the two magnets is considered fixed to the ground, while the other is placed at a fixed distance h, referred to as the gap distance, in the direction of magnetization (**J** or **J'**). Along the orthogonal direction to the magnetization (in this case x), the magnet assumes then variable relative positions, identified with $\Delta_x$. The interaction force is then evaluated by varying $\Delta_x$ for different values of the gap distance $h$. This system is subsequently implemented in the experimental setup.

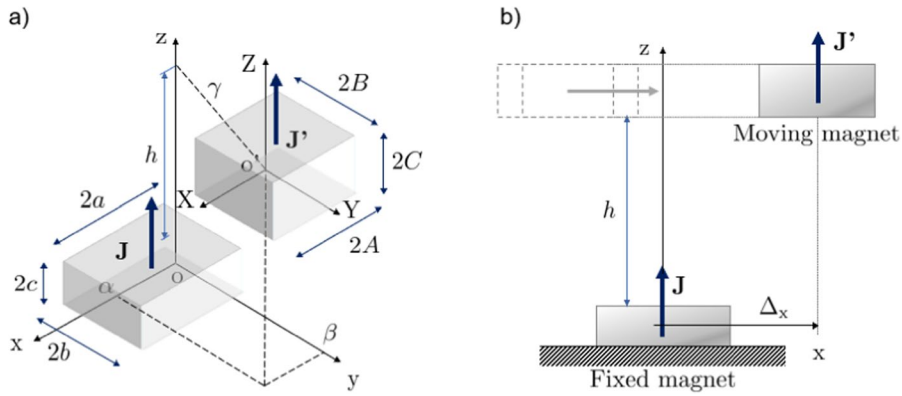


**Fig. 2** Schematic of the interacting magnets (**a**) and view in the xz plane with the indication of the typical configuration of relative positions assumed in the study (**b**)

### 3.2.1 *Evidence of the phenomenon*

First of all, the phenomenon is numerically investigated. Two values of shielding thickness t= 0.5 mm and 1.0 mm are initially considered, and the focus is placed only on the x-component of the magnetic force, considering the reference system in Fig. 2. Indeed, magnetic plucking is mainly connected to the force component that is orthogonal to the magnetization vectors. The magnetizations between the central magnet and the shielding are always parallel but the magnetization of the latter is opposite to that of the magnet to which it is attached. Numerical simulations for different gap distances are presented in Fig. 3. As can be seen in each of the plots, by inserting the shielding, a sharpening of the force-distance curve can be obtained, which is an effect of the introduced multiple sign inversion. Compared with the unshielded case, it is also noticeable that as the gap decreases, the force peak is larger. In contrast, as the gap increases the force decreases. However, the sharpening effect is always present, as indicated by the black arrows in Fig. 3. Numerical simulation confirms that the technique also works by shielding only one of the two magnets. As an example, the case for gap distance 1.0 and 1.5 mm and shielding thickness t=1 mm is shown in Fig. 4. By comparing Fig. 4a with Figs. 3b and 4b with Fig. 3c, respectively, one observes that the force-distance curve is sharpened in both cases, even though the presence of single shielding involves smaller peaks of the magnetic force. The experiments comprehend both the configuration with two shielded magnets (denoted by 2 S) and the case of single shielded magnets (denoted by S). In the case of two shielded magnets (2 S), both are composed like the one represented in Fig. 1d, and they interact with parallel and opposite magnetizations. In the case of one shielded magnet (S), one magnetic system is composed like the one in Fig. 1d, while the other is similar to that shown in Fig. 1c, again with parallel and opposite magnetizations.

### 3.2.2 *Comparison with analytical formulas and experiments*

Having conceptually investigated the effect of adding magnetic material polarized in opposite direction to a main magnet through numerical simulation, in the following experimental validations are reported. Furthermore, the modified analytical model is also considered to verify its response also in the case of shielding.

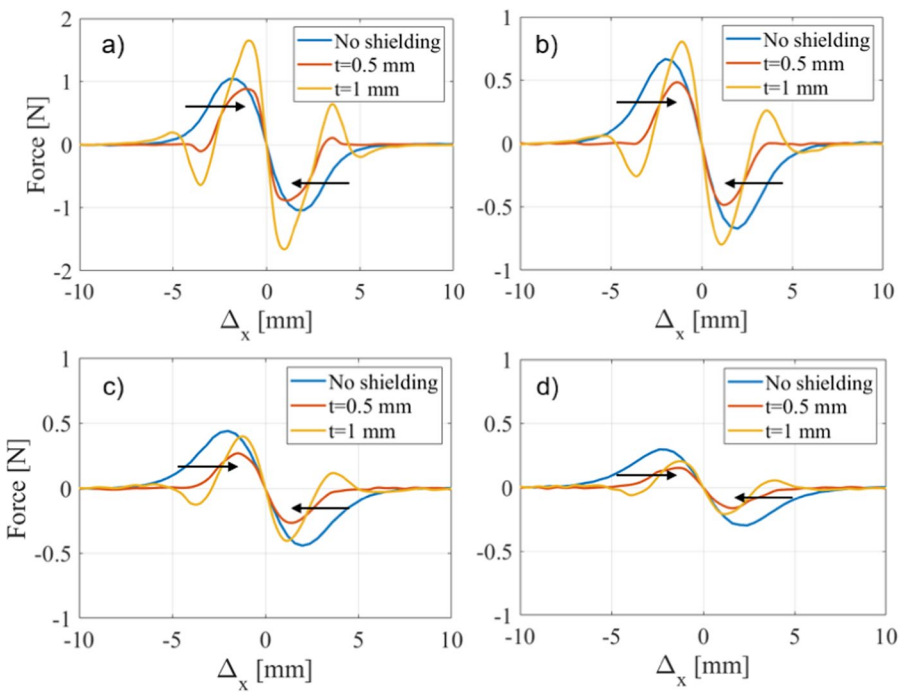


**Fig. 3** Finite element simulations of the magnetic force with two shielded magnets and varying gap distance: **a** 0.5 mm, **b** 1.0 mm, **c** 1.5 mm, and **d** 2.0 mm. The black arrows indicate the versus of the sharpening with respect to the relative distance

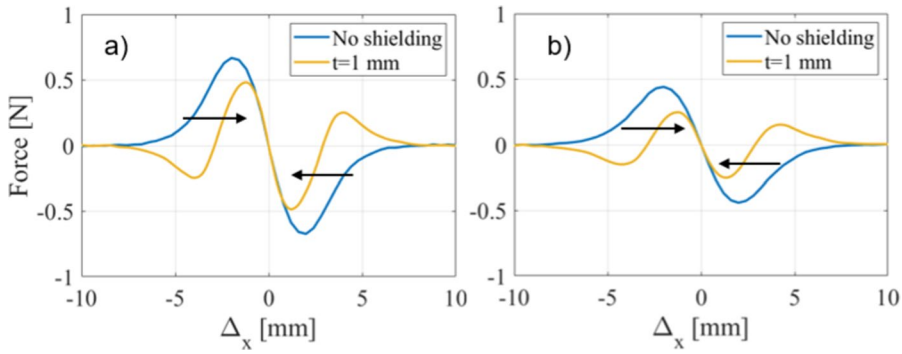


**Fig. 4** Finite element simulations of the magnetic force with one shielded magnet and varying gap distance: **a** 1.0 mm, **b** 1.5 mm. The black arrows indicate the versus of the sharpening with respect to the relative distance

The experimental setup is shown in Fig. 5. It consists of a handcrafted actuator to drive one magnet, a displacement sensor to measure its motion, a load cell S2 Tech 514QD to measure the magnetic force (full-scale FS=30 N, repeatability error: $\leq \pm 0.033\%$ FS, total error: $\leq \pm 0.023\%$ FS, sensitivity: 2 mV/V/FS). The acquisition system is a DAQ Card TM-6062E by National Instruments (12-bit resolution, maximum sampling rate of 500 kHz). The gap distances between the magnets (i.e. $h$ in Fig. 2) is set through a mechanical gauge. To carry out the experiment, one magnet is attached to the rigid rod of the actuator along its motion axis, and the other one to the load cell. Both magnets are not directly attached to the actuator and on the cell, they have been glued with cyanoacrylate onto two Aluminum (i.e. nonmagnetic) rods to avoid magnetic interaction with the supporting equipment.

The velocity of the actuator is fixed at 0.5 mm/s. The analytical formula has been extended to the case of shielded magnets. The shielding is discretized to a finite number of parallelepiped permanent magnets, and each of them interacts with all the others in the layout. Excluding inherent nonlinearities of the ferromagnetic material, justified by the fact that NdFeB is *hard*, the resulting force is the superposition of the various interactions.

The comparison of the results between the analytical solution, the experiments, and the numerical simulation are reported in Fig. 6 for the case with two shielded magnets, and in Fig. 7 for one shielded magnet. In all cases, the experimental curve corresponding to the case without shielding (in red) is also reported, to highlight the effective sharpening of the force-distance curve if the shielding

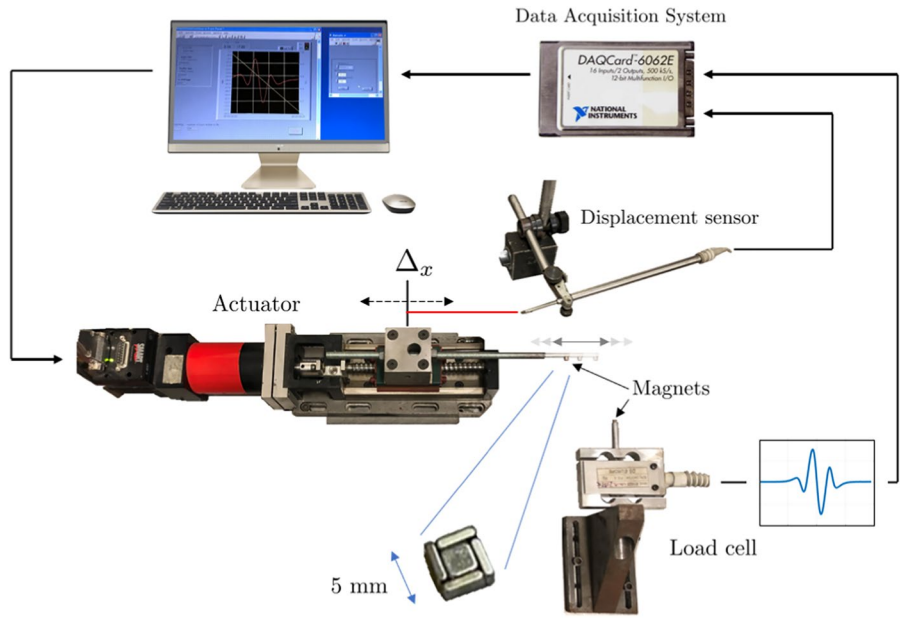


**Fig. 5** Experimental apparatus used to measure the force-distance curves

technique (single or double) is adopted. Considering the results of the case with two shielded magnets for different gap distances, in Fig. 6, it can be seen that the sharpening effect is experimentally confirmed (Exp 2 S), with respect to the unshielded case (Exp. NS), taken from [33]. The increase of the peak force as the gap distance decreases is also experimentally confirmed (e.g. Fig. 6a, b, and also c). The concept is therefore validated. Considering then the comparison with the numerical (FE 2 S) and analytical (An. 2 S) simulation, it emerges that the experimental phenomenon (Exp 2 S) is in good agreement with the computations. In terms of peak forces, the response is always very good, some discrepancy arises in the actual position of the sign reversal for relative position $\Delta_x$ around $\pm 5$ mm. Such a fact is certainly attributable to the real form of the magnetic interaction which is very complex and difficult to capture numerically. Slight shape discrepancies emerge even in the absence of shielding. The analytical formula and the finite element simulation are always in excellent agreement among them and this allows one to use the analytical formula to carry out parametric analyses with a low computational cost. In the experimental data, a slight asymmetry is also observed, essentially due to the inevitable imperfections of the handcrafted setup.

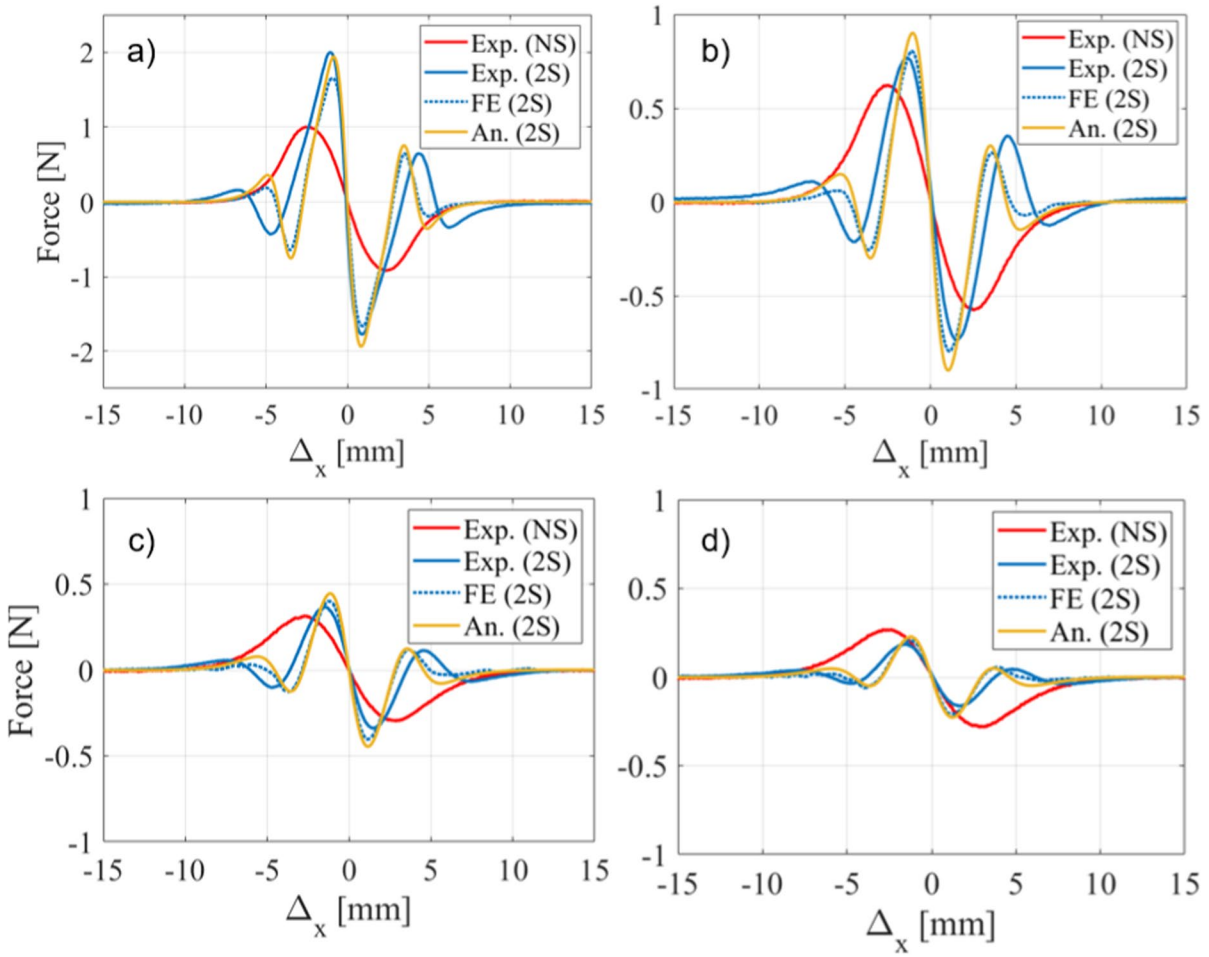


**Fig. 6** Comparison of the experimental magnetic forces with finite element and analytical simulations in case of two shielded magnets and varying gap distance: **a** 0.5 mm, **b** 1.0 mm, **c** 1.5 mm, and **d** 2.0 mm. Exp. (NS): experimental no shielding; Exp. (2 S): experimental double shielding; FE (2 S): finite element double shielding; An. (2 S): Analytical double shielding

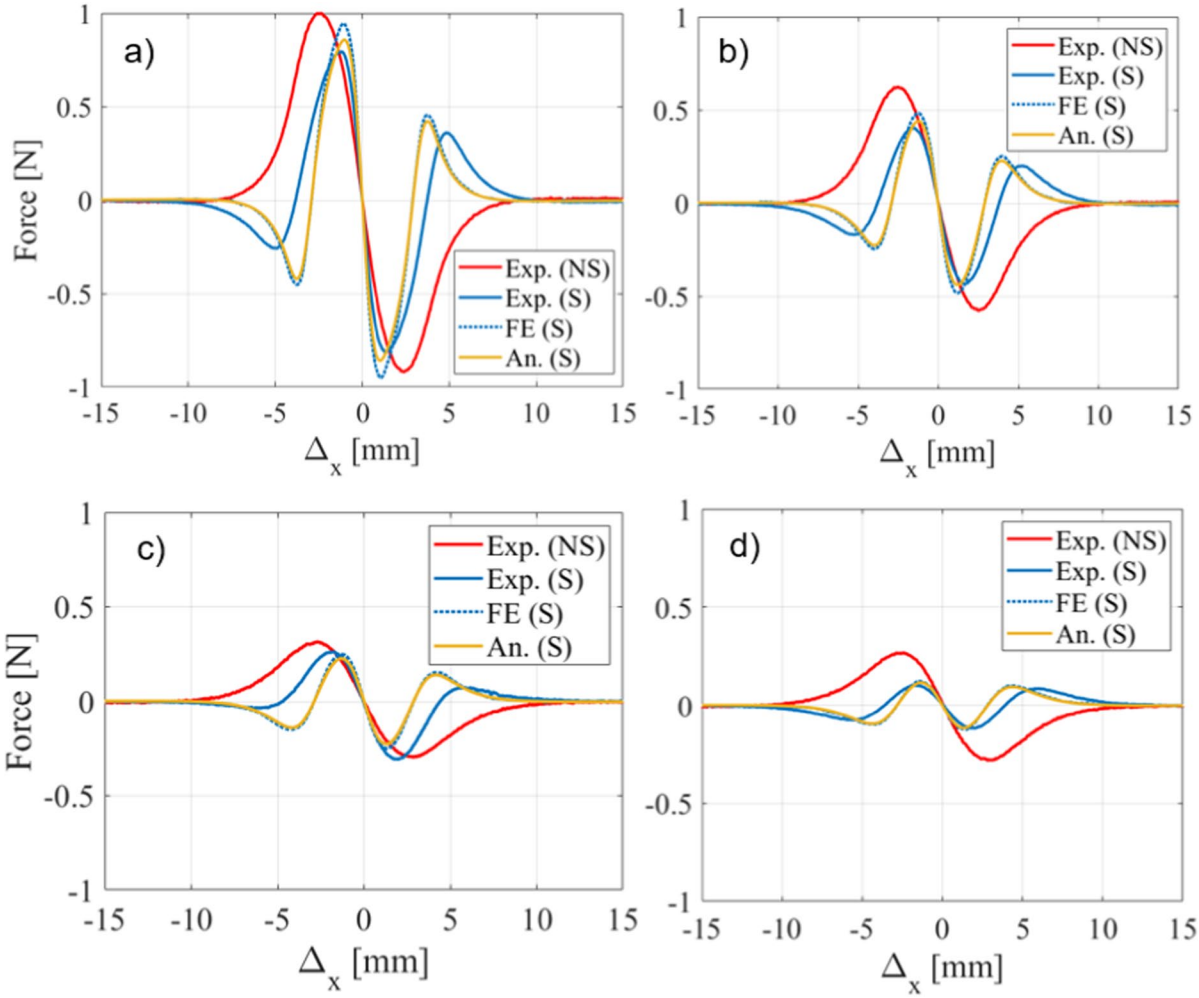


**Fig. 7** Comparison of the experimental magnetic forces with finite element and analytical simulations in case of one shielded magnet and varying gap distance: **a** 0.5 mm, **b** 1.0 mm, **c** 1.5 mm, and **d** 2.0 mm. Exp. (NS): experimental no shielding, Exp. (S): experimental single shielding, FE (S): finite element single shielding, An. (S): Analytical single shielding

Similar observations can be made in the case of a single shielded magnet, considering the plots in Fig. 7. Comparing the experimental data for the shielded and the unshielded cases, the sharpening is always present. However, unlike the double-shielded case, the increase in peak force due to the decrease in gap distance is not observed with respect to the unshielded case. Instead, a decrease in the peak force is also observed for increasing gap $h$, (see Fig. 2). Also taking into account what was observed in the case with double shielding, the fact can be explained as follows. The increase in peak force is due to the fact that in the presence of two shieldings, more magnetic material contributes to the localization of the magnetic field. On the other hand, as the gap increases, a decrease in the peak is always observed with respect to the unshielded case. As the distance increases, the local effect introduced by the shielding vanishes and only the net magnetization of the engineered block is appreciated. This latter takes into account the alternation of signs, leading to an overall decrease.

Having proven a good agreement between the experiments, the numerical simulation, and the analytical one, it is possible to use the latter approach to perform parametric analyses of the force. Such

analyses encompass a varying shielding thickness in the range [0;1] mm for the four gap distance values previously considered. Figures 8 and 9 show the results for double and single shielding, respectively. The graphic aspect of the surfaces shows that the double shielding leads to force-distance curves always much sharper than adopting a single shielding. These surfaces also allow one to appreciate the peak force trend in the shielding thickness, which is in general nonlinear.

## 4 Application to vibration energy harvesting

The concept of magnetic shielding is now applied to the nonlinear dynamics of a piezoelectric vibration energy harvester. The scheme to be considered is represented in Fig. 10. A piezoelectric bimorph with a tip magnet is triggered through magnetic interaction by a moving mass also equipped with a magnet. The mass is externally driven, at constant velocity $\bar{v}$. The nonlinear constitutive model with consideration of elastic hysteresis and nonlinear coupling proposed in [36] is assumed for the piezoelectric material. Ferroelectric hysteresis, on the other hand, is not considered since typically in energy harvesting, the electric field in the piezoelectric layers is well below the coercive value. The focus of the following simulations is on the effect that the technique can provide on the nonlinear dynamic response of the oscillator. The configuration is assumed repulsive between the main (central) magnets since it provides a bistable system, more interesting for energy harvesting [33].

A lumped parameter model is adopted, as suggested in [33, 35]. The transducer is modeled with linearized kinematics, being typically very stiff, and the Euler-Bernoulli beam theory is adopted. Only two degrees of freedom (dofs) are assumed: $U$ for the displacement of the cantilever tip and $V$ for the voltage across the electrodes. A resistive load $R$ is supposed to be connected to the harvester, and the piezoelectric layers are connected in series. The nonlinear second-order differential system governing the problem is the following:

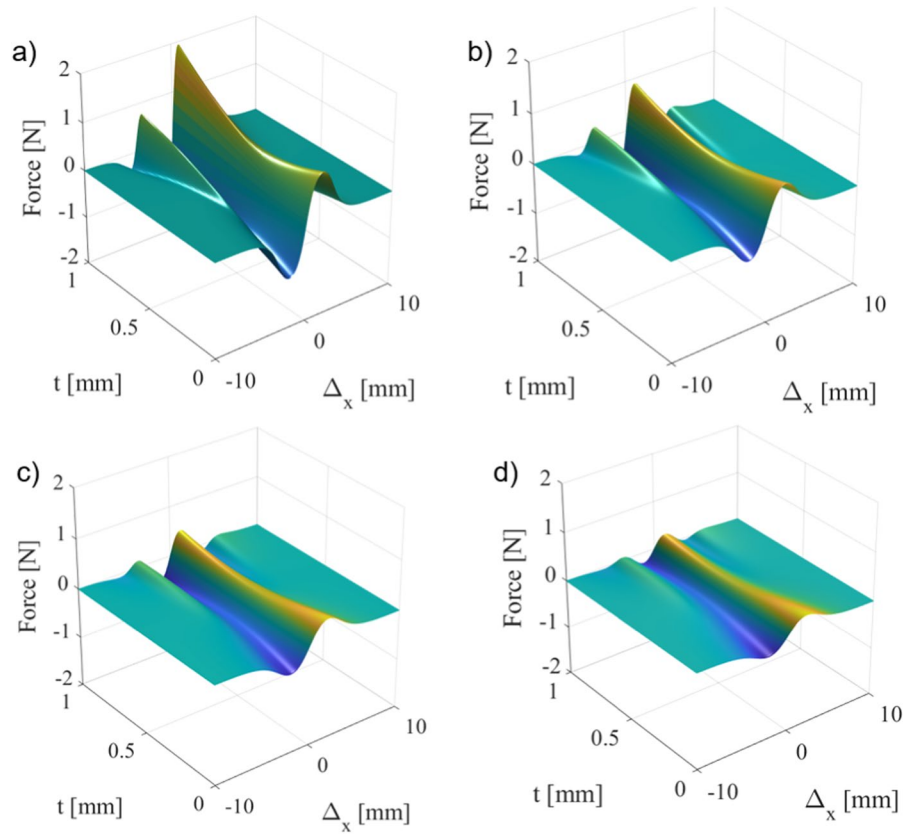


**Fig. 8** Parametric analysis of the magnetic force exerted between two shielded magnets by means of the Yonnet formula. Various gap distances: **a** 0.5 mm, **b** 1.0 mm, **c** 1.5 mm, and **d** 2.0 mm

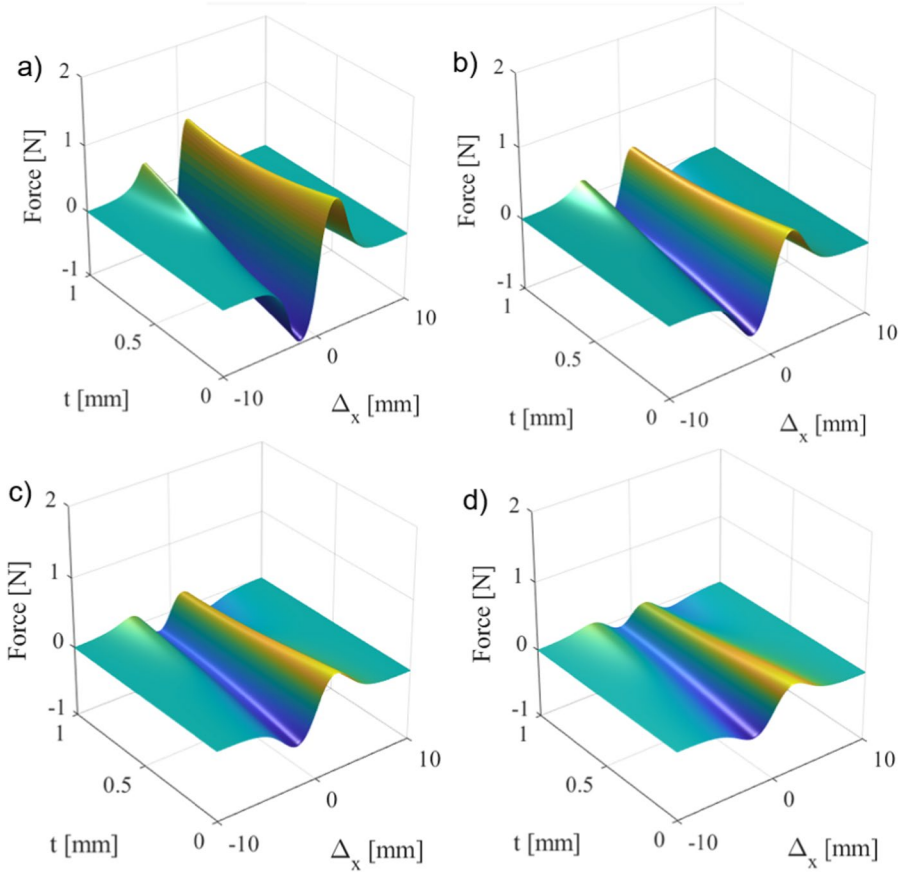


**Fig. 9** Parametric analysis of the magnetic force exerted between two magnets by means of the Yonnet formula, in which just one is shielded. Various gap distances: **a** 0.5 mm, **b** 1.0 mm, **c** 1.5 mm, and **d** 2.0 mm

$$\begin{cases} m\ddot{U} + \left[b_1 U \operatorname{sgn}(U) + b_2 U^2\right] \operatorname{sgn}(\dot{U}) + k_1 U + k_2 U^2 \operatorname{sgn}(U) + \\ -\left[\theta_1 + \theta_2 U \operatorname{sgn}(U)\right] V = F_{mag}(U, \bar{v}) \\ C\dot{V} + \frac{V}{R} + \left[\theta_1 + \theta_2 U \operatorname{sgn}(U)\right] \dot{U} = 0 \end{cases} \tag{2}$$

The coefficients of the system (2) are computed as integral over the volume of the structure. $m$ is the modal mass of the first mode, $b_1$, $k_1$ $\theta_1$ are the linear damping, stiffness, and coupling coefficients, respectively. The coefficients $b_2$, $k_2$, and $\theta_2$ are the nonlinear ones. $C$ is the effective capacitance of the transducer. Extensive details on the modeling calculations can be found in [36] and [37]. $F_{mag}$ is the magnetic force whose variation is caused by the relative motion between the moving mass and the cantilever tip. However, since the mass is supposed to be driven externally at a constant velocity, its dynamics does not appear in the system (2). This system has been implemented in a MATLAB® program and is integrated with the ODE23s solver [38]. To perform numerical simulations, the same data used in [37] are assumed for the materials. All physical and geometrical characteristics are summarized in Table 1.

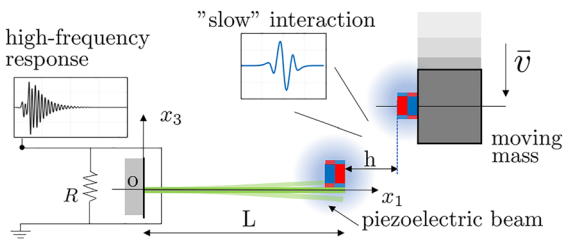


**Fig. 10** Schematic of the energy harvesting principle

In the following simulations, a gap distance between the magnets equal to 0.5 mm is assumed. Two magnetic force patterns are considered:

- the unshielded case in which the magnets have the size equal to $5 \times 5 \times 3\text{mm}^3$,
- the shielded case with the same layout as the previous sections. A central cubic magnet with a side

of 3 mm is covered with opposite polarized hard ferromagnetic material 1 mm thick ($t$ in Fig. 1b).

With this layout, it is possible to compare fairly the performance, using the same amount of magnetic material and having identical frequency of vibration. Three cases of electric circuits have been considered: the arbitrary value of $R$=100 kΩ just to have a comparison also in terms of power, short circuit ($R$=0), and open circuit ($R \longrightarrow \infty$). In the short circuit, the effect of the resistor is zero and it can be seen that the technique works on a purely mechanical oscillator. In the same way, in the open circuit, it can be seen that the technique works as well even when the stiffening effect provided by the resistor is maximum [39].

**Table 1** Geometrical features and material parameters of the harvester

| Parameter | Value | Description |
|---|---|---|
| $b$ | 3.16 mm | cantilever width |
| $L$ | 24.0 mm | cantilever length |
| $L^*$ | 31.8 mm | overhang length |
| $h_p$ | 0.265 mm | PZT layer thickness |
| $h_b$ | 0.990 mm | Brass layer thickness |
| $\rho_p$ | 7800 kg/m$^3$ | PZT mass density |
| $c_{11,p}$ | 66 GPa | PZT Young's modulus |
| $c_{111,p}$ | − 60 TPa | PZT nonlinear elastic constant |
| $e_{31}$ | − 11.6 C/m$^2$ | PZT linear piezoelectric constant |
| $e_{311}$ | − 20 kC/m$^2$ | PZT nonlinear piezoelectric constant |
| $\varepsilon_{33}$ | 14.6 nF/m | PZT dielectric constant |
| $\rho_b$ | 8500 kg/m$^3$ | Brass mass density |
| $c_{11,s}$ | 100 GPa | Brass Young's modulus |
| $b_1$ | 1.70e1 N/m | Linear damping coefficient |
| $b_2$ | 9.00e5 N/m$^2$ | Nonlinear damping coefficient |

Figures 11, 12, 13 show the phase portrait of the nonlinear response for the three aforementioned circuit conditions, in case of a single plucking with $\bar{v} = 0.8$ m/s (reasonable for human motion), without (a) and with (b) the shielding. The benefit of the technique in terms of vibration is clear: the shielded cases describe much larger orbits, in terms of displacements and velocities, which in the shielded case is even higher than the unshielded case. With a resistance of $R$=100 kΩ and a shielded magnet (Fig. 11b), the orbits are clearly discernible owing to the further damping effect of the electrical circuit. In cases of short circuit (Fig. 12) and open circuit (Fig. 12), the system experiences less damping, resulting in a significantly denser appearance of the orbits, which remain larger compared to the unshielded scenario. Figure 14 shows the different dynamics over time. Figure 15 shows the trend of the simulated instantaneous power for $R = 100\,\text{k}\Omega$, in case of absent (a) or present (b) shielding at the same input velocity. With the proposed solution, the results show a gain in terms of peak power of about 17 times. The technique has also been simulated for velocities lower than 0.8 m/s, within the range of 0.2–0.7 m/s, which are pertinent to human motion applications. Figure 16 illustrates the comparison of phase portraits between the unshielded harvester (a) and the shielded one (b). The observations made at 0.8 m/s (Figs. 11, 12, 13, 14, 15) are further corroborated at lower velocities. Specifically, at 0.2 m/s, both cases exhibit a quasi-static regime, characterized by the absence of the structural mode in the dynamic response. However, a higher voltage is attained in the shielded case, attributed to the sharper force-distance curve, although not reported here for conciseness. At 0.3 m/s, the unshielded harvester remains quasi-static, while the shielded case displays high-frequency vibrations, compared

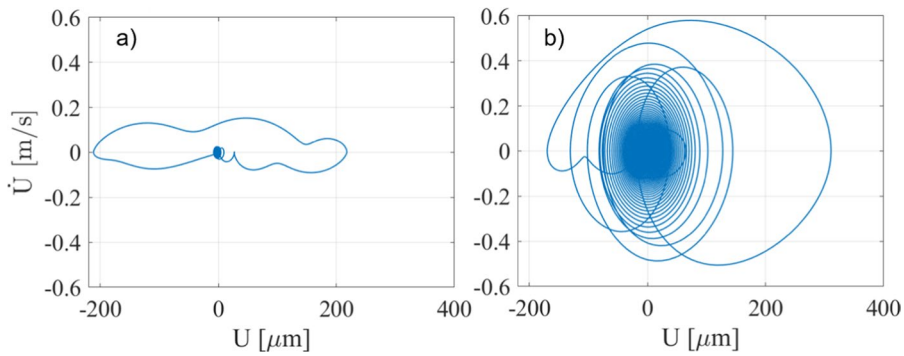


**Fig. 11** Simulated phase portrait of the system with $R = 100\,k\Omega$ for unshielded (**a**), and shielded (**b**) cases

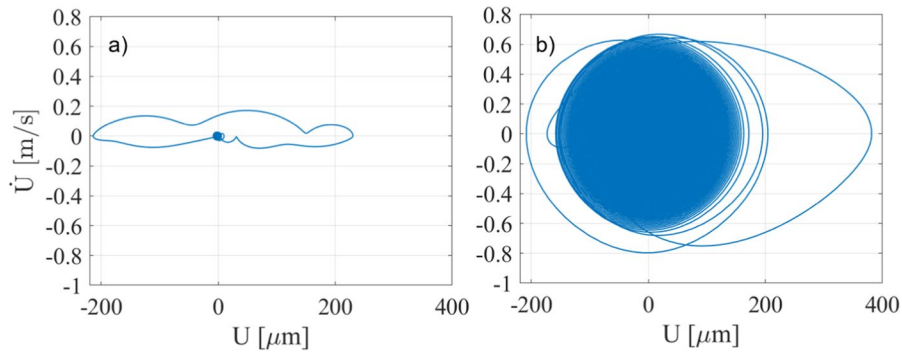


**Fig. 12** Simulated phase portrait of the system in short circuit condition ($R = 0$) for unshielded (**a**), and shielded (**b**) cases

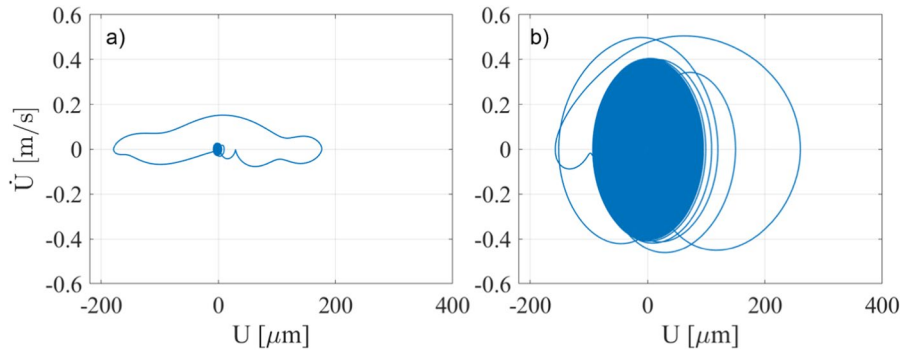


**Fig. 13** Simulated phase portrait of the system in open circuit condition (R$\longrightarrow \infty$) for unshielded (**a**), and shielded (**b**) cases

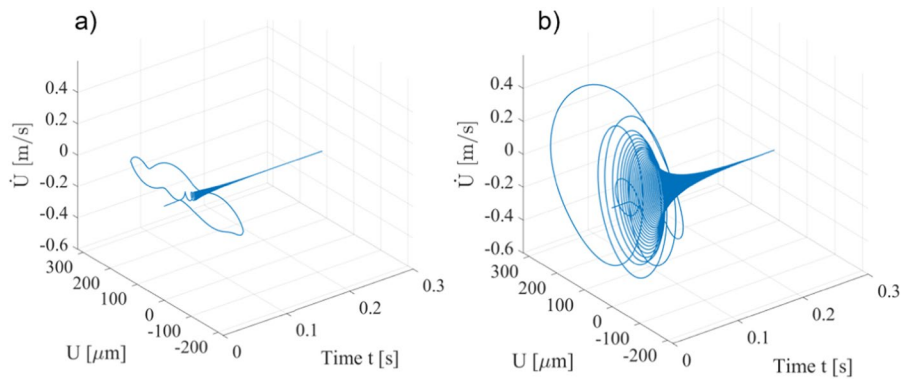


**Fig. 14** Simulated phase portrait of the system with $R = 100\,k\Omega$ for unshielded (**a**), and shielded (**b**) cases, over time

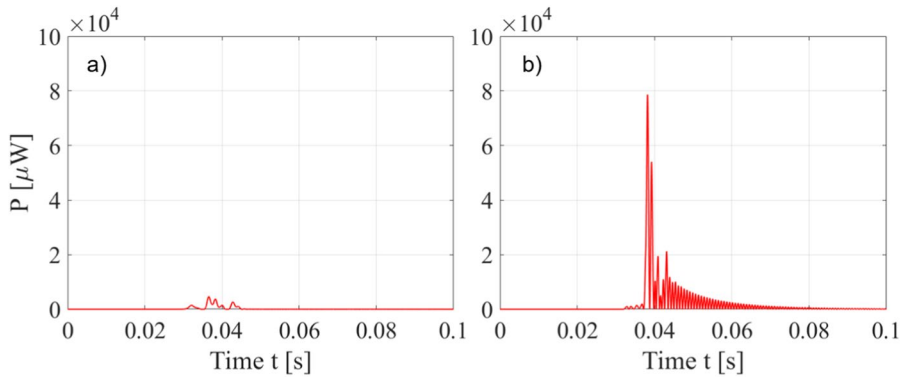


**Fig. 15** Simulated istantaneous power in time domain with $R = 100k\Omega$ for unshielded (**a**), and shielded (**b**) cases, over time

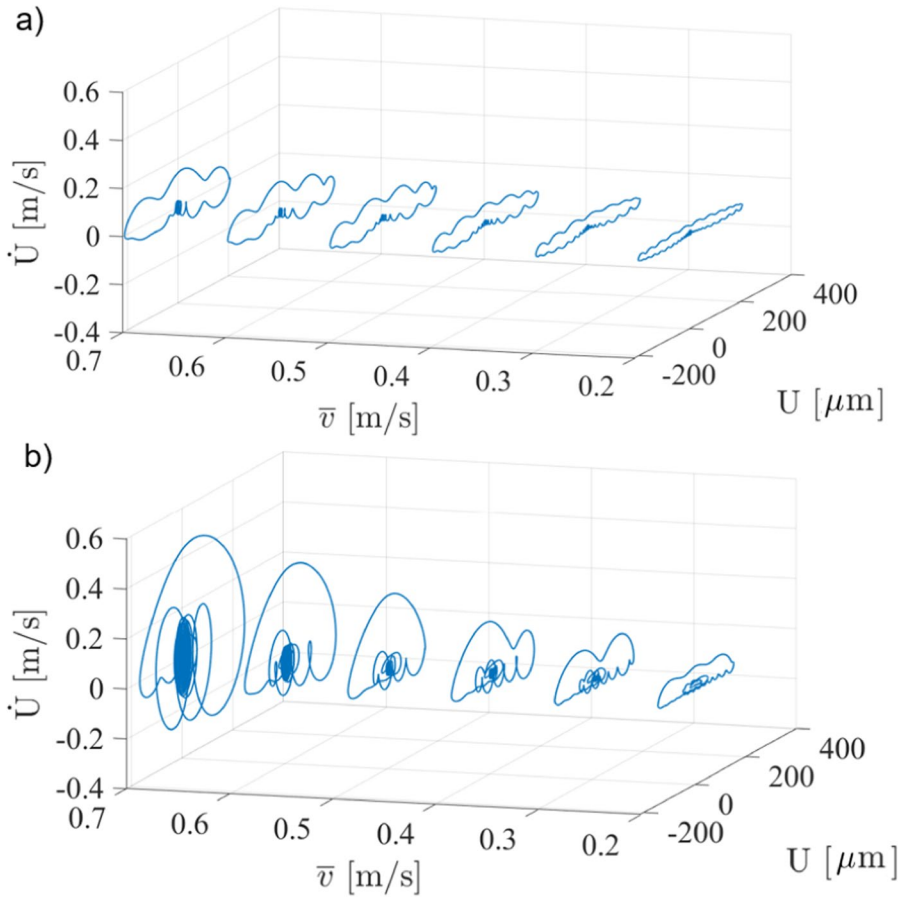


**Fig. 16** Simulated phase portraits of the system with $R = 100k\Omega$ for unshielded (**a**), and shielded (**b**) cases, for different values of interaction velocity $\bar{v}$: 0.2 m/s, 0.3 m/s, 0.4 m/s, 0.5 m/s, 0.6 m/s, 0.7 m/s

to the unshielded counterpart. At 0.4 m/s, even the unshielded harvester initiates oscillations, albeit with minimal displacements, velocities, and voltages when compared with the shielded case. This trend persists across velocities of 0.5 m/s, 0.6 m/s, and 0.7 m/s. It is important to emphasize that the space-dependent force, with assigned fixed velocity, illustrates the concept of the operational principle, through a realistic example of piezoelectric harvester. Since the moving magnet is externally driven, further motion laws, such as harmonic or band-limited colored noise, would not change the conceptual outcome of this research. The parameter influencing the dynamic response is the interaction velocity [37]. For completeness, Table 2 summarizes the simulated performance results with system (2) across the entire velocity range considered (0.2–0.8 m/s). The table allows for a comparison of the results for the cases with and without shielding in terms of RMS voltage ($V_{RMS}$), peak power ($P_p$), and average power ($P_m$). The latter is calculated using Joule's law across the resistor, with the RMS voltage computed from a single plucking of the beam ($P_m = V_{RMS}^2/R$). Peak power is particularly useful for illustrating how the impulsiveness of the phenomenon increases with shielding as velocity increases, from approximately 5.5 times for the slowest case of 0.2 m/s up to about 17 times for the fastest case of 0.8 m/s. Across the entire velocity range considered, the more impulsive dynamics of the shielding case consistently ensure better performance compared to the unshielded case.

## 5 Conclusions

In this work, a new technique in the field of magnetic frequency up-conversion of energy harvesters (or oscillators in general) has been presented. Experiments and simulations have shown that the magnetic force between permanent magnets can be

**Table 2** Simulated RMS voltage ($V_{RMS}$), peak power ($P_p$), and mean power ($P_m$) for different velocities $\bar{v}$ of the moving magnet in the range 0.2–0.8 m/s

| | Unshielded case | | | Shielded case | | |
|---|---|---|---|---|---|---|
| $\bar{v}$ [m/s] | $V_{RMS}$[V] | $P_p$[μW] | $P_m$[μW] | $V_{RMS}$[V] | $P_p$[μW] | $P_m$[μW] |
| 0.2 | 1.61 | 214.27 | 26.08 | 1.86 | 1201.73 | 34.44 |
| 0.3 | 1.77 | 525.48 | 31.40 | 2.20 | 3331.44 | 48.49 |
| 0.4 | 2.01 | 996.48 | 40.22 | 2.49 | 5944.76 | 62.20 |
| 0.5 | 2.22 | 1544.99 | 49.40 | 2.75 | 11047.84 | 75.46 |
| 0.6 | 2.42 | 2417.69 | 58.80 | 3.65 | 23052.12 | 133.19 |
| 0.7 | 2.60 | 3447.75 | 67.47 | 5.24 | 39480.87 | 274.43 |
| 0.8 | 2.78 | 4660.33 | 77.08 | 8.83 | 78613.08 | 779.99 |

manipulated in the space domain. This manipulation occurs by shielding one or more main magnets with additional magnetic material polarized in the opposite direction to the main magnet. With the proposed technique, it is therefore possible to realize dynamic forcing with an intentionally designed impulsiveness. The technique is highly useful where there is a need for an efficient frequency up-conversion in a low-velocity context (e.g. $< 1$ m/s), as in the case of human motion. A computational study carried out on a bimorph piezoelectric harvester, has shown that for a relative velocity between the magnets of 0.8 m/s with a 100 kΩ resistor, there is a 17x gain in terms of peak power for the shielded case. In the considered velocity range, the shielding technique consistently yields superior performance in terms of power compared to the case without shielding. Moreover, the flexibility of the technique extends its applicability also in sensing and actuation context.

**Acknowledgements** MR, FM, AC, and RA acknowledge the support of the H2020 FET-proactive project MetaVEH under Grant Agreement No. 952039. All the authors wish to thank Marco Cucchi of "Laboratorio Prove e Materiali" at Politecnico di Milano for his technical support on the experimental setup.

**Author Contributions** Conceptualization, MR and RA; methodology, all the authors; software, MR, SC, FM; numerical simulations, MR, SC, FP; validation, MR; data curation, MR; resources, RA; writing—original draft preparation MR, SC, AC, RA; visualization, MR; funding acquisition, RA; supervision, RA, AC.

**Funding** Open access funding provided by Politecnico di Milano within the CRUI-CARE Agreement.



## References

1. Roundy S, Wright PK (2004) A piezoelectric vibration based generator for wireless electronics. Smart Mater Struct 13(5):1131
2. Glynne-Jones P, Tudor MJ, Beeby SP, White NM (2004) An electromagnetic, vibration-powered generator for intelligent sensor systems. Sensors Actuat A 110(1–3):344–349. https://doi.org/10.1016/j.sna.2003.09.045
3. Roundy S, Wright PK, Pister KSJ (2002) Micro-electrostatic vibration-to-electricity converters. In: Proceedings of IMECE'02, 2002 ASME international mechanical engineering congress & exposition, pp 487–496, New Orleans, Lousiana, (United States), https://doi.org/10.1115/IMECE2002-39309.
4. Saadon S, Sidek O (2011) A review of vibration-based MEMS piezoelectric energy harvesters. Energy Convers Manage 52:500–504. https://doi.org/10.1016/j.enconman.2010.07.024
5. Anton SR, Sodano HA (2007) A review of power harvesting using piezoelectric materials (2003–2006). Smart Mater Struct 16:3. https://doi.org/10.1088/0964-1726/16/3/R01
6. Clementi G, Cottone F, Di Michele A, Gammaitoni L, Mattarelli M, Perna G, López-Suárez G, Baglio S, Trigona C, Neri I (2022) Review on innovative piezoelectric materials for mechanical energy harvesting. Energies 15:6227. https://doi.org/10.3390/en15176227
7. Maamer B, Boughamourac A, Fath El-Babd AMR, Francis LA, Tounsi F (2019) A review on design improvements and techniques for mechanical energy harvesting using piezoelectric and electromagnetic

schemes. Energy Convers Manage 199:111973. https://doi.org/10.1016/j.enconman.2019.111973
8. Beeby SP, Tudor MJ, White NM (2006) Energy Harvesting Vibration Sources for Microsystems Applications. Meas Sci Technol 17:R175–R195. https://doi.org/10.1088/0957-0233/17/12/R01
9. Galchev T, Kim H, Najafi K (2011) Micro power generator for harvesting low-frequency and nonperiodic vibrations. J Microelectromech Syst 20:4
10. Rosso M, Ardito R (2023) A review of nonlinear mechanisms for frequency up-conversion in energy harvesting. Actuators 12(12):456. https://doi.org/10.3390/act12120456
11. Liu H, Lee C, Kobayashi T, Tay CJ, Quan C (2012) Piezoelectric MEMS-based wideband energy harvesting systems using a frequency-up-conversion cantilever stopper. Sens Actuat A 186:242–248. https://doi.org/10.1016/j.sna.2012.01.033
12. Pozzi M, Min SHA, Zhu M, Jones RK, Goulermas JY (2012) The Pizzicato knee-joint energy harvester: characterization with biomechanical data and the effect of backpack load. Smart Mater Struct 21:75023–75030. https://doi.org/10.1088/0964-1726/21/7/075023
13. Priya S (2005) Modelling of electric energy harvesting using piezoelectric windmill. Appl Phys Lett 87:184101. https://doi.org/10.1063/1.2119410
14. Rastegar JS, Murray RT (2010) Novel two-stage piezoelectric-based electrical energy generators for low and variable speed rotary machinery. In: Proceedings of SPIE—the international society for optical engineering, San Diego, California (United States), https://doi.org/10.1117/12.847755
15. Pillatsch P, Yeatman EM, Holmes AS (2013) Magnetic plucking of piezoelectric beams for frequency up-converting energy harvesters. Smart Mater Struct 23:025009. https://doi.org/10.1088/0964-1726/23/2/025009
16. Pozzi M (2016) Magnetic plucking of piezoelectric bimorphs for a wearable energy harvester. Smart Mater Struct 25:045008. https://doi.org/10.1088/0964-1726/25/4/045008
17. Fu H, Yeatman EM (2019) Rotational energy harvesting using bi-stability and frequency up-conversion for low-power sensing applications: Theoretical modelling and experimental validation. Mech Syst Signal Process 125:229–244. https://doi.org/10.1016/j.ymssp.2018.04.043
18. Fu H, Mei X, Yurchenko D, Zhou S, Theodossiades S, Nakano K, Yeatman EM (2021) Rotational energy harvesting for self-powered sensing. Joule 5(5):1074–1118. https://doi.org/10.1016/j.joule.2021.03.006
19. Rolanas D, Arunas K, Valdas G (2018) Analysis of magnetic plucking dynamics in a frequency up-converting piezoelectric energy harvester. Smart Mater Struct 27:085016. https://doi.org/10.1088/1361-665X/aac8ad
20. Rosso M, Nastro A, Baù M, Ferrari M, Ferrari V, Corigliano A, Ardito R (2022) Piezoelectric energy harvesting from low-frequency vibrations based on magnetic plucking and indirect impacts. Sensors 22(15):5911. https://doi.org/10.3390/s22155911
21. Rosso M (2024) Intentional and inherent nonlinearities in piezoelectric energy harvesting. Springer Cham. https://doi.org/10.1007/978-3-031-51046-5
22. Janphuang P, Lockhart RA, Isarakorn D, Henein S, Briand D, de Rooij NF (2015) Harvesting energy from a rotating gear using an AFM-Like MEMS piezoelectric frequency up-converting Energy Harvester. J Microelectromech Syst 24:3. https://doi.org/10.1088/0964-1726/25/4/045008
23. Wen H, Zhang X, Ye H, Yan Y (2021) Research on the mechanism of magnetic flux concentrator in the gap-to-gap induction heating of wind power gear. Int J Thermal Sci 168:107055
24. Mrozek K, Muszyński P, Poszwa P (2021) Application of magnetic concentrator for improvement in rapid temperature cycling technology. Polymers. https://doi.org/10.3390/polym13010091
25. Bao L, Wang B, You X, Li H, Gu Y, Liu W (2020) Numerical and experimental research on localized induction heating process for hot stamping steel sheets. Int J Heat Mass Transfer. https://doi.org/10.1016/j.ijheatmasstransfer.2020.119422
26. Gao K, Qin X, Wang Z, Zhu S, Gan Z (2016) Effect of magnetizer geometry on the spot induction heating process. J Mater Process Technol 231:125–136. https://doi.org/10.1016/j.jmatprotec.2015.12.028
27. Sun X, Jang L, Pong PWT (2013) Magnetic flux concentration at micrometer scale. Microelectron Eng 111:77–81
28. Maspero F, Catani G, Cuccurullo S, Bertacco R (2021) MEMS magnetometer using magnetic flux concentrators and permanent magnets. In: 2021 IEEE 34th international conference on micro electro mechanical systems (MEMS), Gainesville, FL, USA. https://doi.org/10.1109/MEMS51782.2021.9375441
29. Chigirinsky S, Kustov M, Dempsey N, Ndao C, Grechishkin R (2009) MEMS magnetometer using magnetic flux concentrators and permanent magnets, calculations and measurements of the magnetic field of patterned permanent magnetic films for lab-on-chip applications. Rev Adv Mat Sci. pp 85–91
30. Rosso M, Kohtanen E, Corigliano A, Ardito R, Erturk A (2022) Dynamical behavior of frequency up-converted piezoelectric vibration energy harvesters at different velocities of magnetic interaction, 2022 21st international conference on micro and nanotechnology for power generation and energy conversion applications (PowerMEMS), Salt Lake City, Utah (United States) https://doi.org/10.1109/PowerMEMS56853.2022.10007622
31. Stanton SC, McGehee CC, Mann BP (2010) Nonlinear dynamics for broadband energy harvesting: investigation of a bistable piezoelectric inertial generator. Physica D 239:640–653
32. Akoun G, Yonnet JP (1984) 3D analytical calculation of the forces exerted between two cuboidal magnets. IEEE Trans Magn 20(5):1962–1964
33. Rosso M, Corigliano A, Ardito R (2022) Numerical and experimental evaluation of the magnetic interaction for frequency up-conversion in piezoelectric vibration energy harvesters. Meccanica 57:1139–1154. https://doi.org/10.1007/s11012-022-01481-0
34. Rosso M, Corigliano A, Ardito R (2021) An investigation on the magnetic interaction for frequency up-converting

piezoelectric vibration energy harvesters. In: 2021 IEEE 20th international conference on micro and nanotechnology for power generation and energy conversion applications (PowerMEMS), Exeter, United Kingdom, https://doi.org/10.1109/PowerMEMS54003.2021.9658373
35. Ardito R, Corigliano A, Gafforelli G, Valzasina C, Procopio F, Zafalon R (2016) Advanced model for fast assessment of piezoelectric micro energy harvesters. Front Mater 3:17. https://doi.org/10.3389/fmats.2016.00017
36. Leadenham S, Erturk A (2015) Unified nonlinear electroelastic dynamics of a bimorph piezoelectric cantilever for energy harvesting, sensing, and actuation. Nonlinear Dyn 79:1727–1743. https://doi.org/10.1007/s11071-014-1770-x
37. Rosso M, Kohtanen E, Corigliano A, Ardito R, Erturk A (2023) Nonlinear phenomena in magnetic plucking of piezoelectric vibration energy harvesters. Sensors Actuat A Phys 362:114667. https://doi.org/10.1016/j.sna.2023.114667
38. Shampine LF, Reichelt MW (1997) The MATLAB ODE suite. SIAM J Sci Comput 18:1–22. https://doi.org/10.1137/S106482759427642
39. Erturk A, Inman DJ (2011) Piezoelectric energy harvesting. Wiley, New York